buildings

MDPI

Article

Experimental Study of Alkali-Activated Cementitious Materials Using Thermally Activated Red Mud: Effect of the Si/Al Ratio on Fresh and Mechanical Properties

Kai Guo [1], Haifeng Dong [2], Junyi Zhang [3], Liqing Zhang [1,2] and Zhiping Li [1,2,*]

[1] State Key Laboratory of Performance Monitoring and Protecting of Rail Transit Infrastructure, East China Jiaotong University, Nanchang 330013, China; guokai@ecjtu.edu.cn (K.G.); zlq@ecjtu.edu.cn (L.Z.)
[2] School of Civil Engineering and Architecture, East China Jiaotong University, Nanchang 330013, China; 2024018085901018@ecjtu.edu.cn
[3] Department of Civil and Environmental Engineering, The Hong Kong Polytechnic University, Hung Hom, Kowloon, Hong Kong, China; jyzhang@alumni.tongji.edu.cn
* Correspondence: lizhiping@ecjtu.edu.cn

Abstract: Bayer red mud (RM)-based geopolymers are economical and ecofriendly alternatives to cement because of their superior performance. This study investigated alkali-activated cementitious materials by combining RM, fly ash (FA) and slag, and the mixtures were used to produce ecofriendly composites. The influence of the Si/Al molar ratio (3.30–3.79) on the initial properties (setting time and flowability) and hardened properties (compressive strength, drying shrinkage and water permeability) of the composite materials was studied. The Na_2O content was fixed at 4 wt%, and the thermal activation temperature was 800 °C. The phase evolution and geopolymerization mechanism of the effect of the initial Si/Al molar ratio on the material properties was investigated by FTIR, XRD, TG–DTG and SEM–EDS. The results of M1.2Si333 indicated that the compressive strength of the blends can reach 33.5 MPa at 28 days, with a drying shrinkage rate of 1.20%. Compressive strength decreases, while drying shrinkage increases with a higher initial Si/Al ratio. Microstructural analyses revealed that a low Si/Al ratio and alkali activator modulus enhance the dissolution of precursors to form C–(A)–S–H gels, which increase the compressive strength. The results promoted the application of RM-based geopolymer-engineered cementitious composite and enhanced the resource efficiency of the bauxite residue.

Keywords: alkali-activated materials; sustainable materials; compressive strength; waste management; geopolymerization mechanism

Academic Editor: Grzegorz Ludwik Golewski

Received: 3 January 2025
Revised: 22 January 2025
Accepted: 27 January 2025
Published: 12 February 2025

Citation: Guo, K.; Dong, H.; Zhang, J.; Zhang, L.; Li, Z. Experimental Study of Alkali-Activated Cementitious Materials Using Thermally Activated Red Mud: Effect of the Si/Al Ratio on Fresh and Mechanical Properties. *Buildings* **2025**, *15*, 565. https://doi.org/10.3390/buildings15040565

1. Introduction

Red mud (RM) is an alkaline solid waste obtained during the extraction of alumina from bauxite ore, primarily through the Bayer process [1]. The stockpiling of RM is increasingly contributing to significant issues, including the occupation of arable land, environmental contamination (such as water, soil and air pollution), and the degradation of the ecological environment [2,3]. The highly alkaline substances and heavy metal ions of RM can infiltrate the soil during rainfall, leading to soil salinization and groundwater contamination, which pose significant threats to the soil environment. Additionally, the dispersed RM particles cause severe contamination of the environment, due to the effects of wind and other influences. To address the issue of RM, it is essential to develop an efficient and environmentally sustainable alternative treatment method to traditional cement. The use of RM as a precursor to produce geopolymer paste composites could be a useful

solution. This method can be realized for two reasons. On the one hand, the naturally high pH of RM, at approximately 13, can help create an alkaline environment that promotes the dissolution of precursors, then accelerating the geopolymerization process [4,5]; on the other hand, RM particles are fine and have a large specific surface area, which means that they can react with alkaline substances such as NaOH and sodium silicate [6]. The small particles can also fill the voids in the mixture, improving the density of the material and thereby enhancing the strength and stability of the geopolymer [7]. Therefore, the potential of RM for the application of solid waste has gained the attention of many researchers.

Resource utilization is imperative in addressing the challenges posed by the large stockpile of RM and its environmental pollution consequences. The utilization of RM mainly revolves around areas such as construction materials and civil engineering [8]. RM is used to develop cement clinkers [9,10] and hybrid alkali-activated foamed concrete [11]; RM is used as a clay alternative for the production of fired bricks [12], artificial aggregates [13,14], and binding materials or additives in cement-based materials [15]; in addition, heavy metal ions are used as fixers in RM-based geopolymers [16] and for packing density in polymeric materials [17]. RM alone cannot develop sufficient strength, because the aluminum and silicon species present in the RM are predominantly in crystalline form, which have low dissolution rates in alkaline environments, indicating that they cannot affect the geopolymerization [18]. Alkali–thermal pretreatment significantly improves the reactivity of the Al and Si components in the RM. Ye et al. [19] demonstrated that the dissolution efficiency of reactive Al and Si from thermally treated RM can be three times higher than that of untreated RM. Hu et al. [20] reported that 800 °C is an optimal calcination temperature for RM. The solubility of aluminosilicate increases, leading to a corresponding rise in reactivity, when the calcination duration is 3 h. They also investigated the effect of increasing the Na_2O content from 0 to 7.5 wt% on the solubility efficiency of SiO_2 and Al_2O_3. Liu et al. [21] investigated a thermal pretreatment applied to five types of RM by heating each sample at 800 °C for 2 h. A significant negative correlation was found between the concentrations of Si, Al and Fe in the thermally treated RM and the mechanical properties of the resulting geopolymer. Thus, alkali–thermal pretreatment is an effective approach to enhance the reactivity of RM [22,23]. Furthermore, the energy consumption for the thermal pretreatment of RM is relatively lower than that required for clinker kilns in cement production [10]. Therefore, ways to improve the reactivity of RM can be activated by alkali–thermal pretreatment.

Recent studies have made significant advancements in the development of geopolymers by using RM. Most of these studies reported relatively high compressive strengths for geopolymers synthesized with Si/Al molar ratios ranging from 3.0 to 5.0 and alkali activator moduli of between 0.5 and 2.0 M [24,25]. These findings indicate that, when the Si/Al molar ratio exceeds this range, the hydration products tend to exhibit lower compressive strengths [26–28]. Li et al. [4] reported that the compressive strength of RM-based geopolymers increased when the alkali activator modulus was below 1.5 M, while the strength decreased as the RM dosage increased. Shi et al. [29] prepared a geopolymer using a RM–blast furnace slag–fly ash (FA) ternary system. With a precursor material ratio of 1:1:2, the 28-day compressive strength reached 27.34 MPa. Thus, the mechanical properties of RM can be examined on the basis of the initial Si/Al molar ratio and alkali activator modulus provided by precursor materials.

In this study, the objective was to synthesize a geopolymer material using RM derived from bauxite through alkali–thermal pre-treatment. The effects of the alkali activator modulus and Si/Al molar ratio on the fresh and hardened properties of RM–FA–ground granulated blast furnace slag (GGBS)-based geopolymer samples were evaluated. The hydration products of alkali-activated thermally activated RM were characterized by XRD, SEM-EDS, FTIR and TG–DTG. The effects of different Si/Al molar ratios and alkali activator moduli on the mechanical properties, hydration characteristics and microstructure of the

RM were observed. When the relationship between macroproperties and microproperties is established, the mechanism behind the improvement in the mechanical properties of alkali-activated thermally activated geopolymers can be revealed, thereby providing practical significance for their application in green cement-based materials.

2. Materials and Methods

2.1. Raw Materials

The alkali activator in this study consisted of an industrial grade sodium silicate ($Na_2O•nSiO_2$) and an analytical grade sodium hydroxide (NaOH). The $Na_2O•nSiO_2$ was obtained from Henan Borun Casting Materials Co., Ltd., with a silica modulus of 2.68 (Na_2O = 11.9%, SiO_2 = 31.9% and H_2O = 56.2%). Firstly, sodium hydroxide was dissolved in water and stirred for 5 min, followed by a 15-min resting period to allow the chemical reaction to take place. Sodium silicate was then added, mixed for another 5 min, and left to rest for 24 h before being combined with the precursor material.

RM, FA and GGBS were used as precursors for the geopolymers. The FA was sourced from Henan Jinrun New Materials Co. Ltd., while the RM and GGBS were supplied by Lingshou Mineral Products Co. Ltd. The RM and GGBS were characterized using X-ray fluorescence (XRF) spectroscopy, with the results presented in Table 1. SEM images of the raw materials are shown in Figure 1. The RM exhibited irregularly shaped particles with rough surfaces, while the GGBS and FA consisted of smooth, polygonal particles. The RM was dried in an oven at 105 °C for 24 h before being ground in a ball mill. Alkali–thermal pretreatment is a common technique for enhancing the reactivity of RM, particularly in the preparation of RM–FA–GGBS-based geopolymers, with 800 °C identified as the optimal calcination temperature, which was attributed to its rich amorphous phase and glassy structure. The geopolymers synthesized from RM activated at 800 °C exhibited the highest compressive strength, characterized by the formation of abundant amorphous clusters and layered gels, which combined to form a dense network structure. Therefore, in this study, the RM was calcined in an autoclave at 800 °C for 3 h, and a ternary composite geopolymer was synthesized by combining RM with FA, while GGBS was added as a calcium source.

Table 1. Chemical composition (wt%) of the RM, FA and GGBS.

Raw Material	Al_2O_3	SiO_2	CaO	Na_2O	Fe_2O_3	TiO_2	Others	LOI
RM	25.11	16.93	6.02	11.60	36.43	1.54	1.70	-
FA	25.67	58.7	4.74	1.94	4.3	1.16	1.74	2.8
GGBS	13.70	31.10	40.90	0.38	0.65	1.26	2.85	0.96

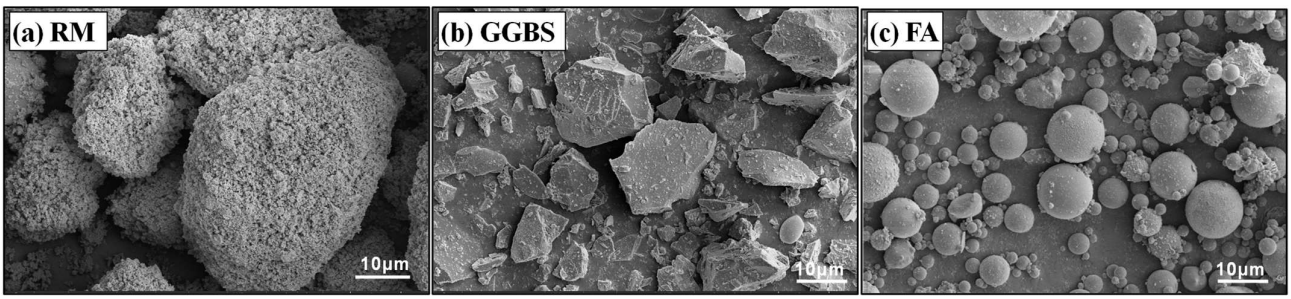

Figure 1. SEM images of RM, FA and GGBS.

2.2. Material Design

Suitable and ecofriendly RM–FA–GGBS-based geopolymers were obtained by classifying these samples into three groups with a constant Na_2O content of 4 wt%. The mixture proportions for the geopolymer samples are provided in Table 2. Three different

RM mixture ratios were tested to examine the effect of the Si/Al ratio on both fresh and hardened properties of the RM–FA–GGBS-based geopolymers. The mass ratios of RM, FA and GGBS were set at 3:5:2, 3:4:3, and 2:5:3, respectively. Additionally, alkali activators with varying alkaline solution (Ms) values were used to adjust the initial Si/Al ratios. The modulus of the Ms was set at 1.2, 1.4, 1.6, and 1.8. A water-to-binder ratio of 0.5 was selected based on trial experiments to ensure good workability in the fresh state. According to previous studies, a Si/Al ratio range of 3.2 to 3.7 was associated with a microstructure characterized by low porosity and high strength in geopolymers. The Si/Al ratio range for the RM-FA-GGBS-based geopolymer was determined to be between 3.33 and 3.79 using the information provided in Table 1 and the SiO_2 content in the sodium silicate solution.

Table 2. Mixture design of thermally activated red mud-based geopolymers.

No.	Alkali Solutions		w/b [a]	Precursors (wt%)				Si/Al [c] Ratio	Remarks
	Modulus [b]	Na_2O (wt%)		RM	Thermally Activated Temperature (°C)	FA	GGBS		
M1.2Si333	1.2	4	0.5	30	800	50	20	3.33	Group 1
M1.4Si339	1.4	4	0.5	30	800	50	20	3.39	
M1.6Si345	1.6	4	0.5	30	800	50	20	3.45	
M1.8Si350	1.8	4	0.5	30	800	50	20	3.50	
M1.2Si330	1.2	4	0.5	30	800	40	30	3.30	Group 2
M1.4Si336	1.4	4	0.5	30	800	40	30	3.36	
M1.6Si342	1.6	4	0.5	30	800	40	30	3.42	
M1.8Si348	1.8	4	0.5	30	800	40	30	3.48	
M1.2Si361	1.2	4	0.5	20	800	50	30	3.61	Group 3
M1.4Si367	1.4	4	0.5	20	800	50	30	3.67	
M1.6Si373	1.6	4	0.5	20	800	50	30	3.73	
M1.8Si379	1.8	4	0.5	20	800	50	30	3.79	

[a] water to binder ratio. [b] alkali activator modulus. [c] silicon to aluminum ratio.

To prepare the binder, the sodium silicate solution, NaOH particles, and water were thoroughly mixed and then cooled to room temperature. The RM was added, followed by FA and GGBS, which were stirred together for 2 min. The composite alkali solution was then gradually poured into the well-blended dry ingredients and mixed for an additional 2 min. After the binder was prepared, its properties were assessed. For the hardened properties, the fresh binder mixture was poured into 40 mm × 40 mm × 40 mm cube molds, and in between each layer, the mixture was tapped with a spatula at least 25 times in two perpendicular directions to eliminate air voids. The molds were then covered with a thin plastic sheet and left to cure at room temperature for approximately 24 h before demolding. After demolding, the samples were stored in a curing room at 20 ± 2 °C and 90 ± 5% relative humidity (RH) until they reached the desired testing ages.

2.3. Experimental Methodology

2.3.1. Fresh Properties

The fresh properties of RM–FA–GGBS-based geopolymers, including setting time and flowability, were evaluated. The setting times of the alkali-activated slag pastes were determined using the Vicat needle method. The paste mixture was cast into a truncated cone mold (φ65 mm × φ75 mm × 40 mm), and the initial setting time was recorded when the needle penetrated the paste to a depth of 4 ± 1 mm from the bottom of the mold after adding the alkaline solution. Following the initial setting test, the mold was inverted for the final setting time test, which was noted when the needle penetrated the paste by no more than 0.5 mm.

The flowability of the fresh paste was assessed using a conical mold. The mold, with a height of 60 mm and inner diameters of 36 mm at the top and 60 mm at the bottom, was

placed on a wet glass plate. After the mold was lifted, the maximum diameters of the paste in two perpendicular directions were measured after 1 min, and the average value was used as an indicator of flowability.

2.3.2. Hardened Properties

The hardened properties of the RM–FA–GGBS-based geopolymers were characterized by compressive strength, drying shrinkage and water permeability. Compressive strength was measured by using a material testing system. The fresh paste was cast into cuboid molds (40 mm × 40 mm × 40 mm) and cured under 90 ± 5% relative humidity (RH) and 20 ± 2 °C for 24 h. After demolding, the samples were further cured until reaching the desired testing ages, with compressive strength tested at 3, 7, and 28 d using a loading rate of 2.4 KN/s.

For the drying shrinkage test, three samples from each mixture were tested. After curing for 1 d, the initial length of the samples was measured using a micrometer, and the samples were then exposed to standard drying conditions. The length change was recorded every 2 d for 28 d. The water permeability of each geopolymer mixture was tested by measuring the water penetration depth. Cylindrical samples (80 mm at the top, 70 mm at the bottom, and 30 mm in height) were subjected to a constant pressure of 0.2 MPa for 1 h at the bottom circular surface, with the top exposed to the atmosphere. The outlet pressure was incrementally increased from 0.1 to 1.5 MPa over several hours, and the depth of water penetration was recorded after rupture.

2.3.3. Microstructural Test

Following compressive strength testing at various ages, the fractured samples were soaked in anhydrous ethanol for 7 d to terminate hydration. They were then dried in a vacuum oven at 60 °C to remove residual moisture. For X-ray diffraction (XRD) analysis, the samples were ground and sieved through a 75 μm mesh. The XRD patterns were recorded at a step size of 5 °/min over a range of 5° to 85°, using Cu–Kα radiation (15 mA/40 kV). Fourier transform infrared (FTIR) analysis was conducted using a spectrometer with a wavenumber range from 450 to 3900 cm^{-1}. Thermogravimetric (TG) and derivative thermogravimetric (DTG) analyses were performed using a thermogravimetric analyzer to identify the main chemical components of the geopolymer composites. Approximately 10 mg of powder (≤75 μm) was heated from room temperature to 800 °C at a rate of 20 °C/min.

For scanning electron microscopy (SEM), approximately 5 mm^3 of the sample was selected, coated with gold, and analyzed using field-emission SEM (equipped with energy dispersive X-ray spectroscopy, EDS) under an acceleration voltage of 5 kV. Energy spectrum analysis was performed at multiple points to assess the microstructure and elemental composition of the samples.

3. Results and Discussion

3.1. Fresh Properties

3.1.1. Setting Time

The setting time of each fresh RM–FA–GGBS-based geopolymer mixture is shown in Figure 2. In the three sets of experiments, the initial setting time and final setting time of the mixtures increased almost linearly with the Si/Al ratio. The initial setting times of the RM-based geopolymer samples ranged from 69 to 175 min, while the final setting times varied between 90 and 248 min. A noticeable rise in both setting times of up to 124.64% for the initial and 122.22% for the final was observed when the Si/Al ratio increased from 3.33 to 3.50 (Figure 2a). This mechanism results from groups 2 and 3 being aligned with group 1 in terms of the setting time. Figure 2b shows the effect of the Si/Al ratio from

3.30 to 3.48 on the initial and final setting times of the geopolymer mixtures. The initial setting time of M1.2Si330 was 81 min. After increasing the Si/Al ratio, the initial setting time of M1.8Si348 was prolonged by 175 min, resulting in a 116.05% increase in the initial setting time. The increase in Al_2O_3 tended to accelerate the solidification of the geopolymer, while the addition of SiO_2 inhibited solidification. The phase transition necessary for the formation of geopolymer gel was hindered in a system with a high initial Si/Al ratio and limited Na_2O content, due to the difficulty in dissolving the raw materials. Furthermore, for RM, FA and GGBS controlled at 2:5:3, the maximum time of 248 min was observed for M1.8Si379, with a Si/Al ratio of 3.79, whereas the minimum time of 111 min was observed for M1.2Si361, with a Si/Al ratio of 3.61 (Figure 2c). When the alkali activator was added to the RM, FA and slag matrix, the Si–O–Si and Al–O–Al in RM, FA and GGBS particles were activated in the highly alkaline environment created by OH− ions in the solution, leading to the formation of C–(A)–S–H and N–(A)–S–H gels [30]. The reason for this is that the Si/Al ratio of the geological polymer increases, accompanied by an extended setting time [31,32]. In alkali-activated systems, as Ms increases, excess SiO_2 causes the condensation rate between silicate species to gradually decrease [33]. Additionally, Na^+ ions interact with silica tetrahedrons, limiting the number of sodium ions available for reaction, which in turn prolongs the setting time [34].

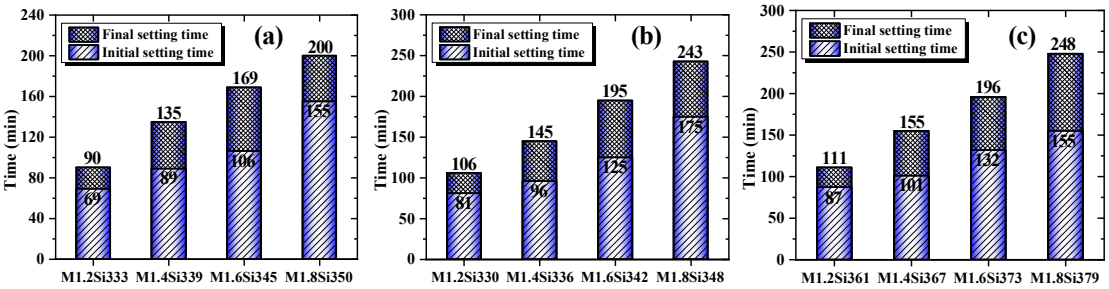

Figure 2. The effect of Si/Al ratio on the setting times of thermally activated red mud-based geopolymers: (**a**) Si/Al = 3.33–3.5, (**b**) Si/Al = 3.30–3.48 and (**c**) Si/Al = 3.61–3.79.

3.1.2. Flowability

The variation in the fluidity of the freshly mixed pastes with different Si/Al ratios of RM–FA–GGBS-based geopolymers is shown in Figure 3. The flowability varied significantly with different mixture ratios. Figure 3a shows that the flowability of the fresh samples increased with increasing Si/Al ratio from 3.33 to 3.50, and the flowability of the geopolymer samples increased from 145 to 205 mm. The viscosity of slurries exhibiting a higher Si/Al ratio was significantly elevated, and this increase in viscosity was correlated with an augmented degree of geopolymerization. However, a higher Si/Al ratio resulted in a reduced degree of geopolymerization, which enhanced the flowability of the RM-FA-GGBS-based geopolymer. Figure 3b shows that the flowability of M1.8Si348 is 45.16%, which is higher than that of M1.2Si330, with measured fluidities of approximately 155 and 225 mm, respectively. Figure 3c shows the effects of a ratio of RM, FA and GGBS of 2:5:3 on the flow properties of RM-based geopolymers. The Si/Al ratio increased the flowability performance of the slurry. When the ratio of Si/Al is 3.61 (M1.2Si361), the slurry had a flowability of 160 mm. The flowability performance of the slurry was best when the ratio of Si/Al doping was 3.79, with the highest flowability of approximately 230 mm. The improvement in flowability retention of the geopolymers can be attributed to two primary factors. Firstly, the smooth spherical morphology of the FA particles enhances the mobility of the constituent materials in the mixture [35]. Secondly, the increase in the Si/Al ratio decreased the amount of sodium hydroxide used, thus decreasing the viscosity of the RM–FA–GGBS-based geopolymer slurry and increasing the flowability of the slurry [36,37].

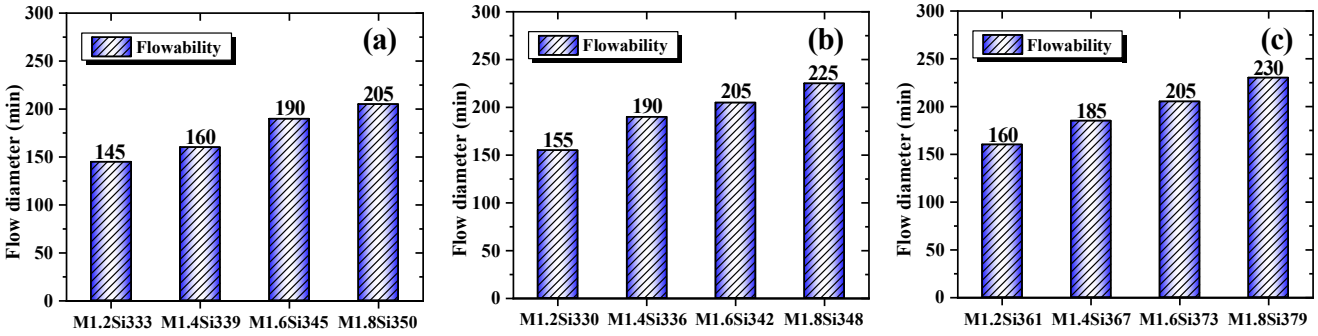

Figure 3. The effect of Si/Al ratio on the flowability of thermally activated red mud-based geopolymers: (**a**) Si/Al = 3.33–3.5, (**b**) Si/Al = 3.30–3.48 and (**c**) Si/Al = 3.61–3.79.

3.2. Hardened Properties

3.2.1. Compressive Strength Development

The 3-, 7- and 28-d compressive strengths of RM-based geopolymer pastes with various ratios of Si/Al are shown in Figure 4. In general, the compressive strength of geopolymers increases when their degree of polymerization is high [38]. All the groups exhibit strengths that increase with increasing curing age. However, the compressive strengths of the three groups of RM–FA–GGBS-based geopolymers gradually decreased with increasing Si/Al ratios from 3.33 to 3.50, from 3.30 to 3.48 and from 3.61 to 3.79, respectively. Figure 4a shows that the 28-d compressive strength of the geopolymer composite material M1.2Si33 reached 33.5 MPa. An increase in the Si/Al ratio can decrease the compressive strength of RM-based geopolymers, and the 3- and 7-d compressive strengths decreased to −34.59% and −29.15%, respectively. In general, geopolymers with low SiO_2/Al_2O_3 ratios also have low crystallinity and porosity; moreover, the greater the compactness, the greater the compressive strength [39]. The $[SiO_4]^{4-}$ and $[AlO_4]^{4-}$ tetrahedrons polymerize to form the geopolymer skeleton, contributing significantly to the compressive strength. However, at higher Si/Al ratios, the alkali gel becomes increasingly unstable [40].

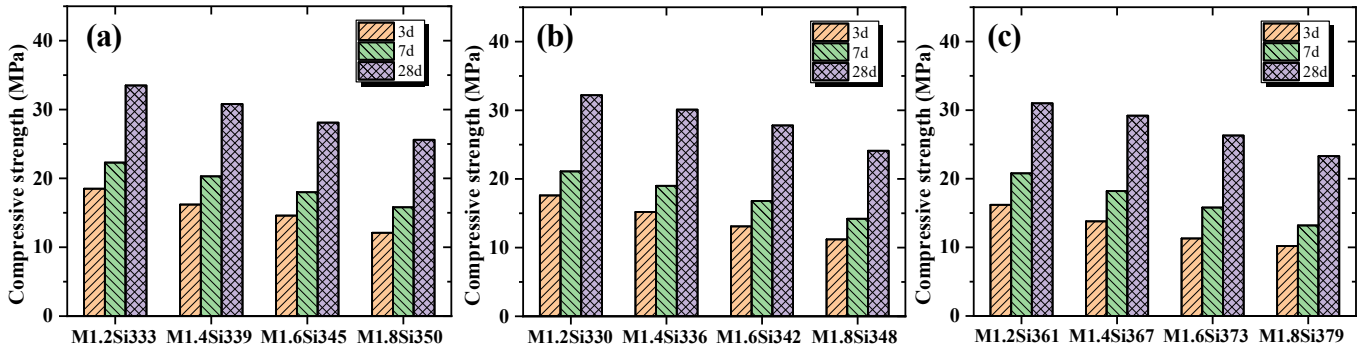

Figure 4. The effect of Si/Al ratio on the compressive strength of thermally activated red mud-based geopolymers: (**a**) Si/Al = 3.33–3.5, (**b**) Si/Al = 3.30–3.48 and (**c**) Si/Al = 3.61–3.79.

When the alkali activator modulus is 1.2 and 1.8, after appropriate alkali activation, the compressive strength can reach a minimum of 24.1 and 32.2 MPa at 28 d, as shown in Figure 4b. At a constant alkali content of 4 wt%, the compressive strength of RM–FA–GGBS-based geopolymers tends to decrease as the silicate modulus increases. Excessive silicate ions from the alkali activator act as polymers, slowing down the dissolution of the precursors and thus reducing compressive strength [41]. An excessively high alkali activator modulus can decrease the dissolution rates of calcium, aluminum and silicate ions, limiting the formation of hydration products [42].

Figure 4c clearly shows that the compressive strength increases with increasing curing age because of the continuous hydration of the precursors. For example, the compressive strength at 28 d for the M1.2Si361 sample was 47.74% higher than that at 3 d and 32.90% higher than at 7 d. The compressive strength of RM–FA–GGBS-based geopolymers at various curing ages primarily depends on the solvated calcium ions in the precursor, which are involved in the formation of strength-enhancing gels like C–(A)–S–H [43].

3.2.2. Drying Shrinkage

Figure 5 illustrates the effects of varying Si/Al ratios on drying shrinkage. In particular, Figure 5a shows that the drying shrinkage of M1.8Si350 (Ms = 1.8) was 35.83% greater than that of M1.2Si333 (Ms = 1.2) in group 1. The drying shrinkage rates of M1.8Si350 and M1.2Si333 were 0.120% and 0.163%, respectively. As illustrated in Figure 5b, under standard curing conditions, the drying shrinkage follows a descending order of M1.2Si330, M1.4Si336, M1.6Si342 and M1.8Si348, with drying shrinkage rates of 0.123%, 0.139%, 0.158% and 0.180%, respectively. Figure 5c shows that the drying shrinkage rates of M1.8Si379 were 49.15%, 32.33% and 15.79% higher than those of M1.2Si361, M1.4Si367 and M1.6Si373, respectively. At a constant alkali content of 4 wt%, the drying shrinkage rate gradually increased with increasing silicate modulus from 1.2 to 1.8. This is largely due to the high silicate modulus, which promotes hydration reactions and increases capillary pressure [44]. At lower Si/Al ratios, the diffusion rate of the hydration products is faster, and the resulting hydration products refine the pore structure and reduce shrinkage [45,46]. The degree of shrinkage is thus greater at higher Si/Al ratios, as the capillary pressure increases [47,48].

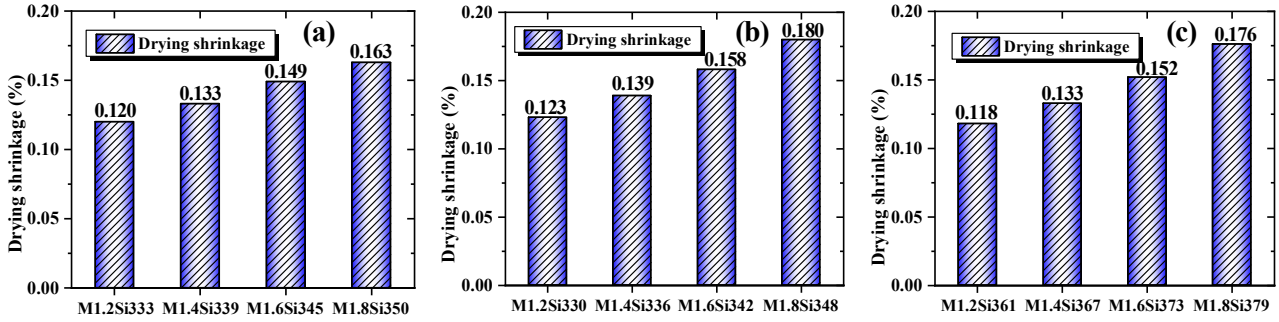

Figure 5. The effect of Si/Al ratio on the drying shrinkage of thermally activated red mud-based geopolymers: (**a**) Si/Al = 3.33–3.5, (**b**) Si/Al = 3.30–3.48 and (**c**) Si/Al = 3.61–3.79.

3.2.3. Water Permeability

Figure 6 shows the impact of varying ratios of Si/Al on the water permeability of RM–FA–GGBS-based geopolymer materials. The results of this study revealed that the permeability increased as the Si/Al ratio increased. In group 3, the water permeability of M1.8Si379, which has a higher Si/Al ratio, was significantly greater than that of M1.2Si361. In the RM–FA–GGBS base geopolymers, an increase in the modulus of the alkali activator led to an increase in permeability. This effect is attributed to the higher modulus of the alkali activator suppressing the synthesis of the C–(A)–S–H gel. With less C–(A)–S–H gel, the pores are insufficiently filled, resulting in a relatively loose structure of the composite material. Consequently, the permeability of the composite material increases [10,49]. This outcome suggests that the increased ratio of Si/Al and the increased modulus of the alkali activator caused the structure of the geopolymers to become sparse, which is consistent with earlier findings related to strength [50].

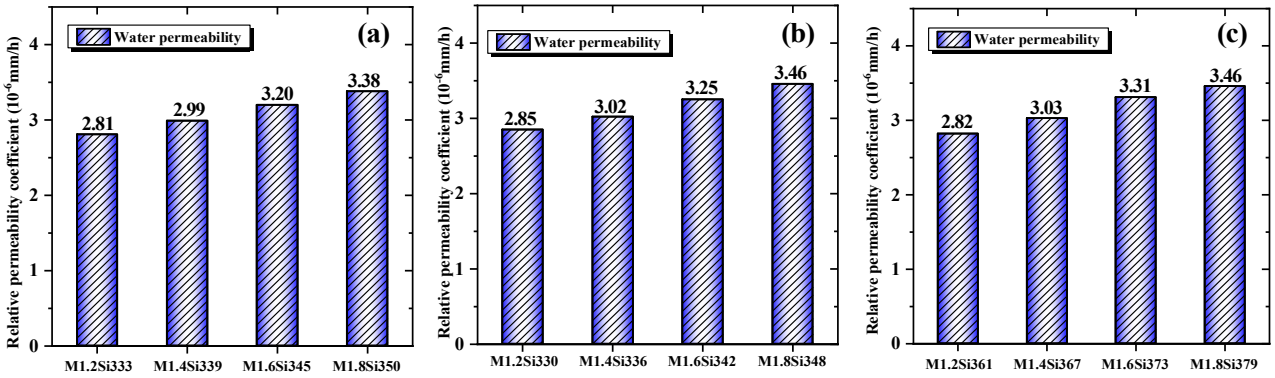

Figure 6. The effect of Si/Al ratio on the permeability of thermally activated red mud-based geopolymers: (**a**) Si/Al = 3.33–3.5, (**b**) Si/Al = 3.30–3.48 and (**c**) Si/Al = 3.61–3.79.

3.3. FTIR and XRD Analysis

Figure 7 shows the FTIR and XRD results of the RM–FA–GGBS-based geopolymer paste composites. The asymmetric stretching and bending vibrations of the –OH bond in bound water cause changes in the peak intensities around 3445 and 1650 cm^{-1}. The peak at approximately 1475 cm^{-1} reflects the O–C–O bond in CO_3^{2-}, which mainly indicates that the geopolymers may have absorbed CO_2 from the air, resulting in the formation of Na_2CO_3 and $CaCO_3$ [51]. Figure 7a–c also show that the geopolymer undergoes carbonation in the air. The primary products of the geopolymerization process are C–(A)–S–H, which appear as Si–O–T (T is Si and Al) bonds in the FTIR spectrum. Transmission peaks are primarily observed in the 1100 to 950 cm^{-1} range [52]. The peak at 453 cm^{-1} corresponds to the Si–O bond [53]. The peak intensity of the Si–O–T bond at approximately 1000 cm^{-1} for M1.2Si333, M1.2Si330 and M1.2Si361 gradually increases. Moreover, as the Si/Al ratio increases from 3.33 to 3.61, the peak position at 1050 cm^{-1} shifts to lower wavenumbers as the reaction progresses, due to the dominance of Si over Al, which causes the asymmetric stretching vibration of the Si–O–T bond to shift downward [54].

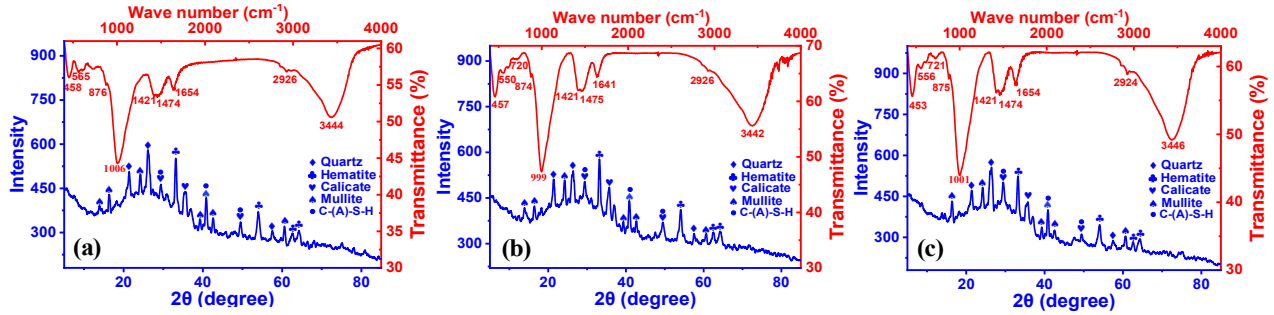

Figure 7. FTIR and XRD curves of thermally activated red mud-based geopolymers (Ms = 1.2): (**a**) M1.2Si333, (**b**) M1.2Si330 and (**c**) M1.2Si361.

The consistent XRD patterns indicate that the mineral phases in all the RM–FA–GGBS-based geopolymers are similar, including quartz, C–(A)–S–H, hematite, calcite, and mullite. The calcite results from carbonation of the $Ca(OH)_2$. The quartz diffraction peak at 26.5° appears in all the XRD patterns, and its intensity decreases with an increasing Si/Al ratio. This is attributed to the higher SiO_2 content involved in the hydration process, leading to more C–(A)–S–H formation, which aligns with the observed increase in compressive strength. Diffraction peaks around 30° and 50° correspond to the C–(A)–S–H gel, suggesting that the geopolymer undergoes polymerization during hydration. Hematite diffraction peaks are also observed in the XRD patterns of samples with higher Si/Al ratios, indicating that these mineral phases in RM are not easily dissolved [55]. At the same time, a small

amount of ettringite is present in the RM geopolymer samples alongside C–(A)–S–H gels and calcite. The intensity of the calcite diffraction peak decreases with the Si/Al ratio, indicating a higher silicon content in the geopolymer pastes, likely leading to an increase in C–(A)–S–H gels [56].

3.4. TG–DTG Analysis

Figure 8 shows the TG–DTG analysis of geopolymer pastes with different initial molar Si/Al ratios. Four distinct heat absorption peaks were observed between 25 °C and 1000 °C. The peak between 100 °C and 200 °C corresponds to the decomposition of bound water in hydration products like AFt gels [57]. The heat absorption peak between 250 °C and 350 °C is attributed to the dehydration decomposition of AH3 [58]. The process involves dehydration of the CFH gel between 600 °C and 700 °C. The peaks between 750 °C and 850 °C correspond to the decarbonation of $CaCO_3$, which forms due to CH carbonation during curing. Differences in water loss temperatures can be linked to variations in the crystallinity of these carbonate minerals [59]. Compared with the M1.2Si330 samples, the M1.2Si361 samples generated more AFt crystals, as indicated by the differences in the 100 °C to 200 °C heat absorption peaks. The enhanced gel formation is primarily due to the increased generation of AFt from geopolymerization at higher Si/Al ratios, leading to improved strength as hydration products fill micropores and create a denser microstructure [60]. Figure 8a also shows that M1.2Si330 has the highest degree of carbonization. The lower the Si/Al ratio, the more easily the alkali solution reacts with CO_2.

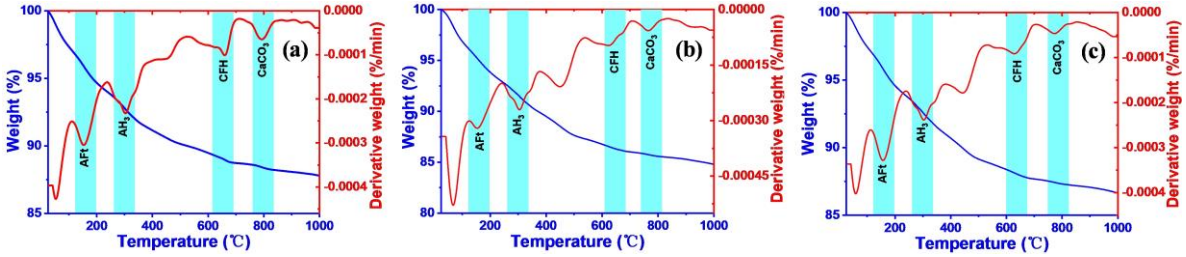

Figure 8. TG-DTG curves of thermally activated red mud-based geopolymers (Ms = 1.2): (**a**) M1.2Si333, (**b**) M1.2Si330 and (**c**) M1.2Si361.

3.5. SEM–EDS Analysis

The microstructural morphology of the RM–FA–GGBS-based geopolymer samples at 28 d was analyzed using SEM–EDS, as shown in Figure 9. At an alkali activator modulus (Ms) of 1.2 (low Si/Al ratio), RM, FA and GGBS fully dissolved and reacted with Ca^{2+} to form a C–(A)–S–H gel, producing a dense structure. The formation of more C–(A)–S–H gel resulted in an even denser material, with reticular and amorphous gel patterns. As seen in Figure 9a, the M1.2Si333 sample exhibited the highest gel density and strength, with interspersed flocculent and fibrous C–(A)–S–H gels. Figure 9b shows that M1.2Si330 and M1.2Si333 had a similar distribution of hydration products but with less C–(A)–S–H gel, alongside some needle-like ettringite crystals [61]. Both M1.2Si330 and M1.2Si333 samples displayed tightly packed nanomicelles in their microstructures. The matrix of M1.2Si330 had a small number of cracks, which resulted in a strength that is relatively low compared with that of M1.2Si333. The M1.2Si333 sample (Si/Al ratio of 3.33) exhibited a significant amount of hydration products on its surface. These hydration products interconnected and filled the gaps, which altered the distribution of pore structure and porosity within the RM–FA–GGBS–based geopolymer. Additional silicon contributed to the formation of salt gel with silicon and aluminum, thereby increasing the compressive strength. The M1.2Si361 sample (Si/Al ratio of 3.61) showed that FA particles are encapsulated by

hydration products on the geopolymer's surface, which hindered further hydration and reduced the compressive strength of the RM–FA–GGBS–based geopolymer [62,63].

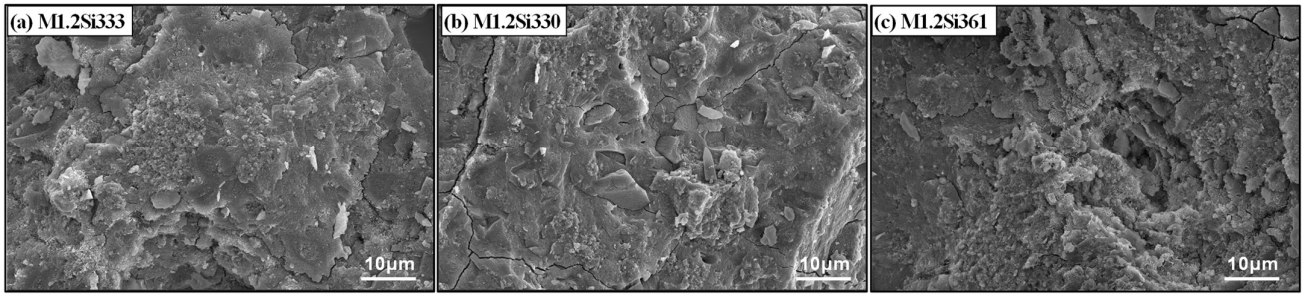

Figure 9. SEM images of thermally activated red mud-based geopolymers (Ms = 1.2).

The elemental distributions of the analyzed RM–FA–GGBS-based geopolymer samples were determined via energy-dispersive X-ray spectroscopy (EDS) (Figure 10). The EDS scanning spectra for M1.2Si333, M1.2Si330 and M1.2Si361 clearly show that the Na, Al and Si distributions in the elemental map intensify where the RM particles are located. Na is predominantly derived from the alkaline activators and is incorporated into the geopolymer structure via ionic coordination with the aluminosilicate framework. A decrease in Na concentration suggests that darker regions in the microstructure correspond to RM particles surrounded by paste, while Ca and Fe are evenly distributed throughout the structure. When the sodium silicate modulus was fixed at 1.2, an increase of the Si/Al ratio led to partial reorganization and decomposition of N-A-S-H gels, which combined with Ca^{2+} in the geopolymers to form C-A-S-H and C-S-H gels. Furthermore, given that the main constituents of the precursors and alkali activator are Si and Al, as previously identified via XRD (Figure 10), the increased Si and Al concentrations in the elemental mapping demonstrated an increased ratio of Si/Al [64].

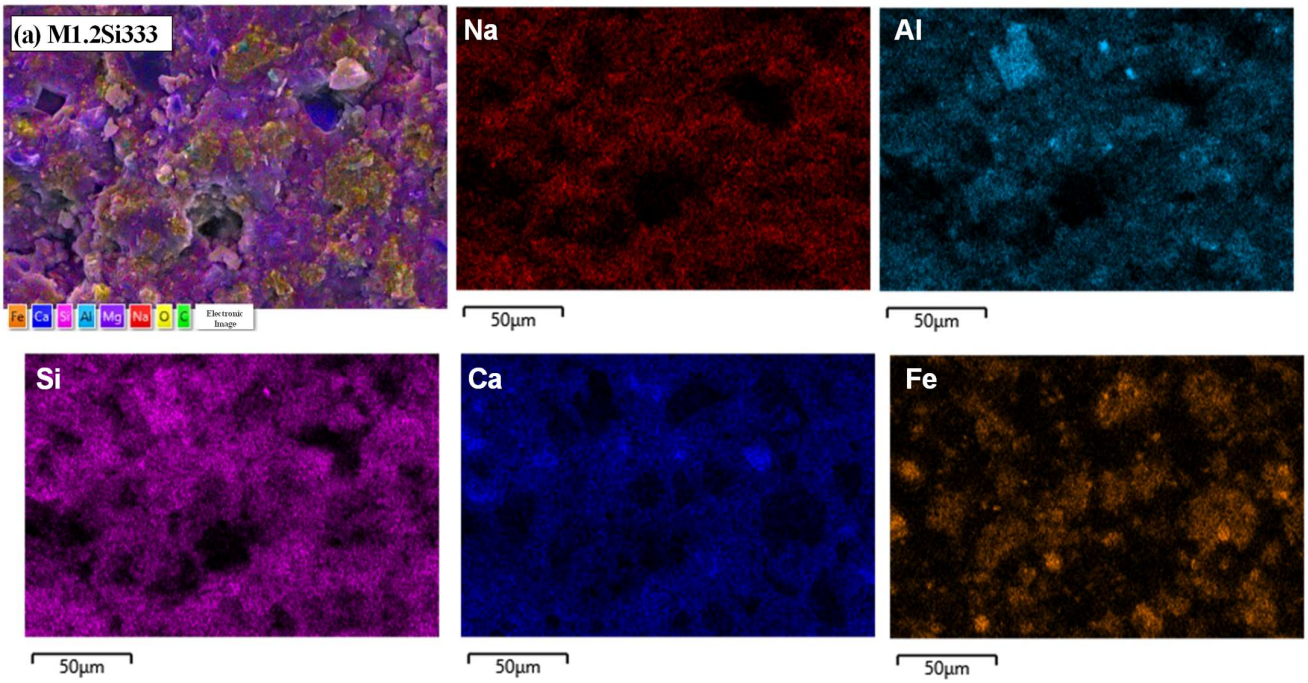

Figure 10. *Cont.*

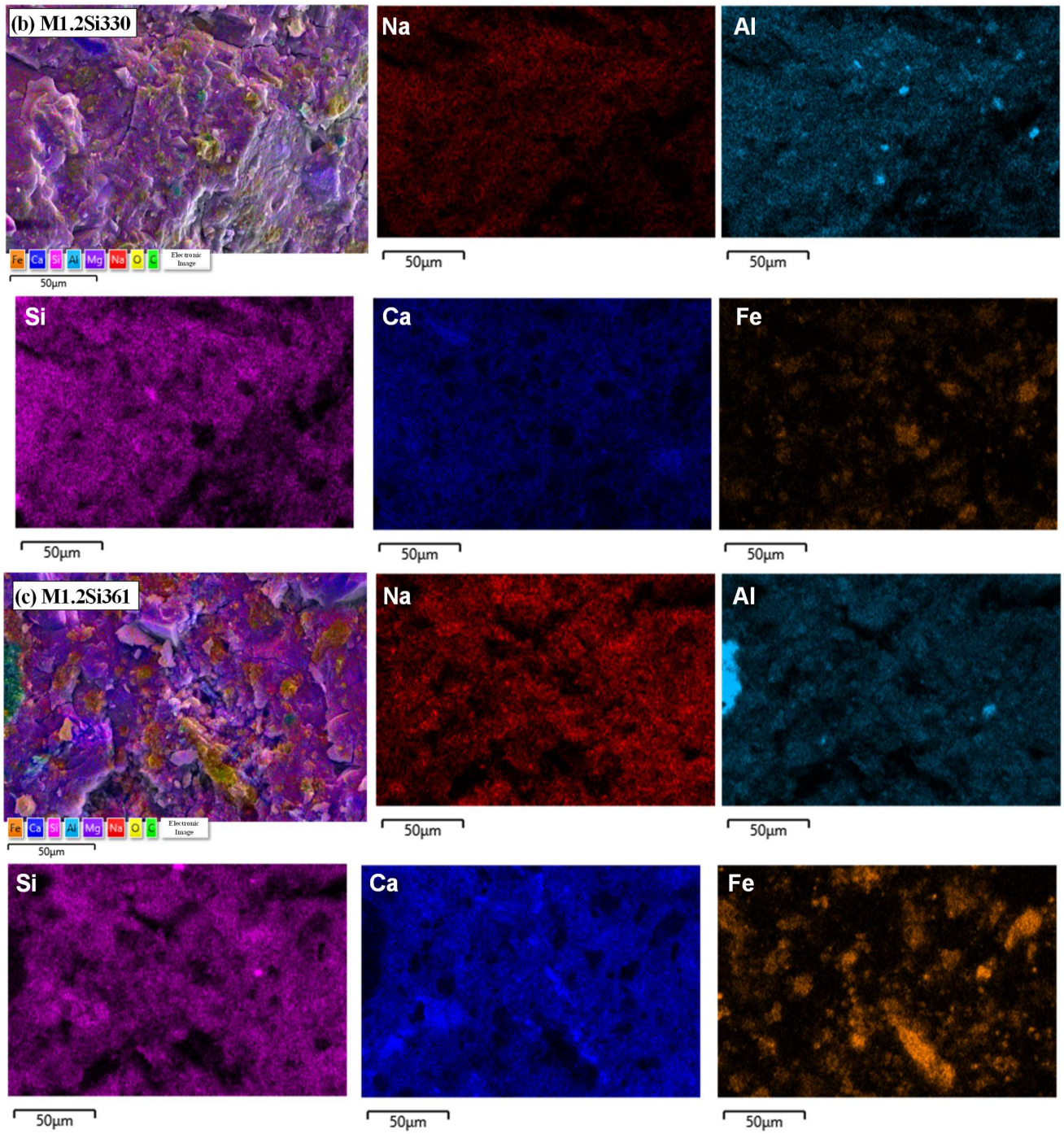

Figure 10. EDS results of thermally activated red mud-based geopolymers (Ms = 1.2).

3.6. Discussion

This study enhances our understanding of hydration reactions during geopolymerization. Since geopolymer formation involves dissolution, reconstruction and polymerization, the Si and Al concentrations influence the type of ion hydrolysis and the condensation process, ultimately affecting the geopolymer's properties. In mixtures with a low Si/Al ratio, aluminum components dissolve more readily than silicon, and the dissolved aluminum species adsorb onto the material, reducing silicon dissolution. As Ca^{2+} dissolves initially, it forms C–S–H, and the availability of $Al(OH)^{4-}$ species promotes the formation of C–(A)–S–H, accelerating precursor dissolution.

Lower Si/Al ratios increase reaction and setting rates, as well as the degree of hydration, which is beneficial for geopolymer production. However, as the Si/Al ratio rises, the

condensation rate between silicate species slows, reducing mechanical properties. This highlights the significant impact of Si/Al ratios on the performance of RM–FA–GGBS-based geopolymers, where lower ratios lead to better fresh and mechanical properties. The RM-FA-GGBS-based geopolymers mixed with 1.2 molar sodium silicate solution (with Si/Al ratios of 3.33 and 3.30, respectively) achieved compressive strength that met the quality standards of load-bearing cement-based materials, while exhibiting minimal drying shrinkage and a denser structure.

The RM geopolymer with a Si/Al ratio of 3.33 showed the highest compressive strength, low shrinkage, and a compact structure, whereas a ratio of 3.79 resulted in the lowest strength (23.3 MPa). Small variations in the Si/Al ratio can drastically affect geopolymer properties, suggesting that increasing Na_2O content may improve mechanical performance at high Si/Al ratios. Moreover, RM-FA-GGBS-based geopolymers exhibited high compressive strength, low water permeability, and low cost characteristics, making them a promising material for replacing cement-based materials and for use in impermeability engineering, which facilitates a win-win scenario for environmental protection and solid waste recycling.

In conclusion, the alkali–thermal activation treatment of RM to prepare RM-FA-GGBS-based geopolymers was an effective technological approach that reduced production costs, decreased carbon emissions, and promoted the sustainable development of construction applications.

4. Conclusions

This study focused on preparing RM–FA–GGBS ternary composites, achieving the synergistic use of RM, FA and GGBS. Firstly, the initial and hardened properties were optimized by adjusting the Na_2O content and the thermal activation temperature. This finding suggests that the Si/Al ratio (3.30–3.79) of RM–FA–GGBS-based geopolymers was regulated by adjusting the RM dosage and the activator modulus, with the Si/Al ratio impacting the fresh properties (setting time and flowability) and hardened properties (compressive strength, drying shrinkage and water permeability) of the geopolymers that were studied. Moreover, the effect of the Si/Al molar ratio on the performance of RM–FA–GGBS-based geopolymers was further analyzed via microscopic tests. On the basis of the results obtained, the following conclusions can be drawn:

(1) An increase in the Si/Al ratio enhanced the setting time and flowability of the mixture, which was attributed to the effects of $[AlO_4]^{4-}$ and $[SiO_4]^{4-}$ from precursor materials and alkali activators on hydration. An optimal Si/Al ratio significantly improved the fresh properties of the material.

(2) The compressive strength of RM–FA–GGBS-based geopolymers decreased, while the drying shrinkage and water permeability increased with an increasing Si/Al ratio from 3.33 to 3.50. At a high Si/Al ratio, the dissolution of silicoaluminate was suppressed, leading to an insufficient concentration of silicoaluminate ions.

(3) The primary hydration products of RM–FA–GGBS-based geopolymers included quartz, C–(A)–S–H, hematite, calcite and mullite. The low Si/Al ratio blends contained a substantial quantity of C–(A)–S–H, which filled the pores, resulting in a relatively dense microstructure and contributing to increased strength.

(4) SEM–EDS characterization revealed that the M1.2Si333 samples exhibited denser microstructures and more hydration products. The low Si/Al ratio resulted in a finer and more homogeneous pore structure in the RM geopolymer, generating additional hydration products that contributed to higher strength.

In general, the results indicated that the effective use of RM, FA and GGBS allowed for the production of geopolymer composites exhibiting suitable fresh and hardened performance. This paper offered a novel research avenue for the effective application of RM-FA-GGBS-based

geopolymer as a low-carbon cementing material. The optimal Si/Al ratio of the geopolymer was determined through the degree of polymerization of the generated C-A-S-H and N-A-S-H gels. Furthermore, exploring the incorporation of other waste materials (such as metakaolin, silica fume and coal gangue) into geopolymer formulations to enhance performance and sustainability will be a key focus of future research.

Author Contributions: Investigation and Data curation, K.G. and H.D.; writing—original draft, Z.L.; writing—review & editing, J.Z. and L.Z. All authors have read and agreed to the published version of the manuscript.

Funding: This work was financially supported by the National Natural Science Foundation of China (Grant Nos. 52368046, 52368031), State Key Laboratory of Performance Monitoring and Protecting of Rail Transit Infrastructure (Grant No. HJGZ2024205), and the Key Research and Development Program of Jiangxi Province in China (Grant Nos. 20240N006, 20224BAB204074).

Data Availability Statement: The original contributions presented in the study are included in the article, further inquiries can be directed to the corresponding authors.

Conflicts of Interest: The authors declare no conflict of interest.

References

1. Khairul, M.A.; Zanganeh, J.; Moghtaderi, B. The composition, recycling and utilisation of bayer red mud. *Resour. Conserv. Recycl.* **2019**, *141*, 483–498. [CrossRef]
2. Cheng, Y.; Jiang, N.; Wang, W.; Jin, L.; Yan, S. Environment assessment of modified red mud utilized in roadbed. *Buildings* **2024**, *14*, 2135. [CrossRef]
3. Yinfang, L.; Chunhua, H.; Lihong, T.; Bitang, Z.; Yimeng, G.; Zhiping, L. Study on Curing Agent Ratio of High Strength Silty Clay-Cement Mixed Soil. *J. East China Jiaotong Univ.* **2023**, *40*, 33–39. [CrossRef]
4. Li, Z.; Liu, X.; Gao, Y.; Zhang, J. Study on the hardening mechanism of bayer red mud-based geopolymer engineered cementitious composites. *Constr. Build. Mater.* **2023**, *392*, 131669. [CrossRef]
5. Li, Z.; Zhang, J.; Lei, Z.; Gao, M.; Sun, J.; Tong, L.; Chen, S.; Wang, Y. Designing low-carbon fly ash based geopolymer with red mud and blast furnace slag wastes performance, microstructure and mechanism. *J. Environ. Manag.* **2024**, *354*, 120362. [CrossRef]
6. He, J.; Jie, Y.; Zhang, J.; Yu, Y.; Zhang, G. Synthesis and characterization of red mud and rice husk ash-based geopolymer composites. *Cem. Concr. Compos.* **2013**, *37*, 108–118. [CrossRef]
7. Hu, Z.; Wyrzykowski, M.; Lura, P. Estimation of reaction kinetics of geopolymers at early ages. *Cem. Concr. Res.* **2020**, *129*, 105971. [CrossRef]
8. Ge, X.; Hu, X.; Shi, C. The long-term development in the micro- and macro-properties of geopolymers made from different fly ashes. *Cem. Concr. Compos.* **2024**, *152*, 105637. [CrossRef]
9. Hertel, T.; Van den Bulck, A.; Onisei, S.; Sivakumar, P.P.; Pontikes, Y. Boosting the use of bauxite residue (red mud) in cement—Production of an fe-rich calciumsulfoaluminate-ferrite clinker and characterisation of the hydration. *Cem. Concr. Res.* **2021**, *145*, 106463. [CrossRef]
10. Li, Z.; Gao, M.; Lei, Z.; Tong, L.; Sun, J.; Wang, Y.; Wang, X.; Ternary, X.J. Ternary cementless composite based on red mud, ultra-fine fly ash, and ggbs: Synergistic utilization and geopolymerization mechanism. *Case Stud. Constr. Mater.* **2023**, *19*, e02410. [CrossRef]
11. Yang, Z.; Zhang, J.; Qin, L.; Chen, T.; Gao, X. Study on the early volume stability of cement-based materials during CO_2 curing. *J. Build. Eng.* **2024**, *95*, 110354. [CrossRef]
12. Pandey, V.; Panda, S.K.; Singh, V.K. Preparation and characterization of high-strength insulating porous bricks by reusing coal mine overburden waste, red mud and rice husk. *J. Clean. Prod.* **2024**, *469*, 143134. [CrossRef]
13. Liu, Y.; Zhang, L.; Xue, B.; Chen, L.; Wang, G.; Wang, J.; Wan, H.; Lin, X.; Zhu, G. Simulation of red mud/phosphogypsum-based artificial soil engineering applications in vegetation restoration and ecological reconstruction. *Sci. Total Environ.* **2024**, *951*, 175656. [CrossRef] [PubMed]
14. Zhang, M.; Zhang, X.; Li, J.; Ma, Y.; Zhu, Z.; Liu, J. Effect of aggregate-to-binders ratio on water resistance of red-mud -modified magnesium phosphate repair mortar. *Buildings* **2024**, *14*, 2174. [CrossRef]
15. Dhasindrakrishna, K.; Pasupathy, K.; Ramakrishnan, S.; Sanjayan, J. Progress, current thinking and challenges in geopolymer foam concrete technology. *Cem. Concr. Compos.* **2021**, *116*, 103886. [CrossRef]
16. Wen, H.; Gao, J.; Yang, Y.; Zhao, M.; Gu, L.; Yu, H.; Liu, E. Effect of red mud on combustion behavior and heavy metal stabilization of refuse derived fuel (RDF). *J. Environ. Chem. Eng.* **2023**, *11*, 111106. [CrossRef]

17. Gameiro, T.; Novais, R.M.; Correia, C.L.; Carvalheiras, J.; Seabra, M.P.; Labrincha, J.A.; Duarte, A.C.; Capela, I. Red mud-based inorganic polymer spheres: Innovative and environmentally friendly anaerobic digestion enhancers. *Bioresour. Technol.* **2020**, *316*, 123904. [CrossRef]
18. Yuan, S.; Duan, D.; Sun, J.; Yu, Y.; Wang, Y.; Huang, B.; Peng, J.; Mohamed, S.; Wang, X. Mechanical, alkali excitation, hydrothermal enhancement of 3D printed concrete incorporated with antimony tailings. *Constr. Build. Mater.* **2024**, *443*, 137610. [CrossRef]
19. Ye, N.; Chen, Y.; Yang, J.; Liang, S.; Hu, Y.; Hu, J.; Zhu, S.; Fan, W.; Xiao, B. Transformations of Na, Al, Si and Fe species in red mud during synthesis of one-part geopolymers. *Cem. Concr. Res.* **2017**, *101*, 123–130. [CrossRef]
20. Hu, Y.; Liang, S.; Yang, J.; Chen, Y.; Ye, N.; Ke, Y.; Tao, S.; Xiao, K.; Hu, J.; Hou, H.; et al. Role of fe species in geopolymer synthesized from alkali-thermal pretreated fe-rich bayer red mud. *Constr. Build. Mater.* **2019**, *200*, 398–407. [CrossRef]
21. Liu, J.; Doh, J.-H.; Ong, D.E.L.; Kiely, F.L. Effect of thermal pretreatment on the reactivity of red mud valorized as aluminosilicate precursor for geopolymer production. *Constr. Build. Mater.* **2024**, *445*, 137943. [CrossRef]
22. Zhou, X.; Geng, Z.; Shi, J. Enhanced passivity of reinforcing steel in cementitious materials with thermally-activated red mud. *Cem. Concr. Compos.* **2024**, *153*, 105696. [CrossRef]
23. Yin, S.; Yan, P.; Li, X.; Wang, Y.; Zhang, X.; Sun, Y.; Chen, C. Experimental study on the strength and microstructure of red mud -based silty sand modified with lime-fly ash. *Buildings* **2024**, *14*, 1336. [CrossRef]
24. De Castro Carvalho, I.; Dai, X.; Kirchheim, A.P.; Da Costa, H.N.; Cabral, A.E.B. Early-age structural build-up and rheological assessment of alkali-activated slag-red clay brick waste pastes: Influence of silica modulus and precursors proportions. *Cem. Concr. Compos.* **2024**, *153*, 105730. [CrossRef]
25. Luo, L.; Yao, W.; Liang, G.; Luo, Y. Workability, autogenous shrinkage and microstructure of alkali-activated slag/fly ash slurries: Effect of precursor composition and sodium silicate modulus. *J. Build. Eng.* **2023**, *73*, 106712. [CrossRef]
26. Dinh, H.L.; Liu, J.; Doh, J.-H.; Ong, D.E.L. Influence of si/al molar ratio and ca content on the performance of fly ash-based geopolymer incorporating waste glass and GGBFS. *Constr. Build. Mater.* **2024**, *411*, 134741. [CrossRef]
27. Kim, G.; Cho, S.; Im, S.; Yoon, J.; Suh, H.; Kanematsu, M.; Machida, A.; Shobu, T.; Bae, S. Evaluation of the thermal stability of metakaolin-based geopolymers according to si/al ratio and sodium activator. *Cem. Concr. Compos.* **2024**, *150*, 105562. [CrossRef]
28. Xi, X.; Zheng, Y.; Zhuo, J.; Zhang, P.; Golewski, G.L.; Du, C. Influence of water glass modulus and alkali content on the properties of alkali-activated thermally activated recycled cement. *Constr. Build. Mater.* **2024**, *452*, 138867. [CrossRef]
29. Xiaoshuang, S.; Yanpeng, S.; Jinqian, L.; Yuhao, Z.; Ruihan, H. Preparation and performance optimization of fly ash- slag- red mud based geopolymer mortar: Simplex-centroid experimental design method. *Constr. Build. Mater.* **2024**, *450*, 138573. [CrossRef]
30. Sas, Z.; Sha, W.; Soutsos, M.; Doherty, R.; Bondar, D.; Gijbels, K.; Schroeyers, W. Radiological characterisation of alkali-activated construction materials containing red mud, fly ash and ground granulated blast-furnace slag. *Sci. Total Environ.* **2019**, *659*, 1496–1504. [CrossRef]
31. De Silva, P.; Sagoe-Crenstil, K.; Sirivivatnanon, V. Kinetics of geopolymerization: Role of Al_2O_3 and SiO_2. *Cem. Concr. Res.* **2007**, *37*, 512–518. [CrossRef]
32. Yangyang, H.; Yinfang, L.; Deyin, S.; Yimeng, G.; Bitang, Z.; Chunhua, H. Study on Permeability and Microscopic Mechanism of Cement-Water Glass Improved Silty Clay. *J. East China Jiaotong Univ.* **2023**, *40*, 32–38. [CrossRef]
33. Zhu, J.; Chen, C.; Wang, X.; Jiu, S.; Chen, Y.; Liu, Y. Alkali activation of rock wool furnace slag: Effects of water glass modulus, Na_2O content, and nano-TiO_2. *J. Build. Eng.* **2024**, *98*, 111338. [CrossRef]
34. Pobłocki, K.; Pawlak, M.; Drzeżdżon, J.; Gawdzik, B.; Clean, D.J. production of geopolymers as an opportunity for sustainable development of the construction industry. *Sci. Total Environ.* **2024**, *928*, 172579. [CrossRef] [PubMed]
35. Xu, L.-Y.; Lao, J.-C.; Qian, L.-P.; Khan, M.; Xie, T.-Y.; Huang, B.-T. Low-carbon high-strength engineered geopolymer composites (HS-EGC) with full-volume fly ash precursor: Role of silica modulus. *J. CO_2 Util.* **2024**, *88*, 102948. [CrossRef]
36. Kim, B.; Kang, J.; Shin, Y.; Yeo, T.-M.; Heo, J.; Um, W. Effect of si/al molar ratio and curing temperatures on the immobilization of radioactive borate waste in metakaolin-based geopolymer waste form. *J. Hazard. Mater.* **2023**, *458*, 131884. [CrossRef]
37. Sun, J.; Zhang, Y.; Wu, Q.; Wang, Y.; Liu, H.; Zhao, H.; Cui, W.; Zhang, W.; Wang, X. 3D printed concrete incorporating waste rubber: Anisotropic properties and environmental impact analysis. *J. Mater. Res. Technol.* **2024**, *33*, 2773–2784. [CrossRef]
38. Timakul, P.; Rattanaprasit, W.; Aungkavattana, P. Improving compressive strength of fly ash-based geopolymer composites by basalt fibers addition. *Ceram. Int.* **2016**, *42*, 6288–6295. [CrossRef]
39. Zakira, U.; Zheng, K.; Xie, N.; Birgisson, B. Development of high-strength geopolymers from red mud and blast furnace slag. *J. Clean. Prod.* **2023**, *383*, 135439. [CrossRef]
40. Zhou, L.; Xu, X.; Wang, Q.; Park, J.; Han, Y.; Guo, L.; Chen, R. Microscopic mechanisms and durability evaluation under freeze-thaw conditions of heavy metal solidification in red mud-slag geopolymer. *J. Environ. Chem. Eng.* **2024**, *12*, 114768. [CrossRef]
41. Zhang, G.; Xu, C.; Wang, D.; Wang, Y.; Sun, J.; Zhu, S.; Morsy, A.M.; Liu, Z.; Wang, X. Machine learning-based modeling of interface creep behavior of grouted soil anchors with varying soil moistures. *Transp. Geotech.* **2024**, *48*, 101299. [CrossRef]

42. Wang, J.; Liu, X.; Zhang, Z.; Liu, Y. Synergistic utilization, critical mechanisms, and environmental suitability of bauxite residue (red mud) based multi-solid wastes cementitious materials and special concrete. *J. Environ. Manag.* **2024**, *361*, 121255. [CrossRef] [PubMed]
43. Ren, G.; Gao, X.; Su, A. Application of sisal fiber powder in ultra-high performance concrete: A renewable material for mitigating autogenous shrinkage. *Constr. Build. Mater.* **2024**, *428*, 136304. [CrossRef]
44. Zhang, M.; Li, W.; Li, M.; Min, Q.; Shen, Y.; Ding, C. Mesoscopic simulation of concrete drying shrinkage with hydration kinetics. *Int. J. Mech. Sci.* **2024**, *283*, 109716. [CrossRef]
45. Krizan, D.; Zivanovic, B. Effects of dosage and modulus of water glass on early hydration of alkali–slag cements. *Cem. Concr. Res.* **2002**, *32*, 1181–1188. [CrossRef]
46. Sun, J.; Tang, W.; Wang, Y.; Yao, X.; Huang, B.; Saafi, M.; Wang, X. Electromagnetic and mechanical performance of 3D printed wave-shaped copper solid superstructures. *J. Mater. Res. Technol.* **2023**, *27*, 6936–6946. [CrossRef]
47. Li, Z.; Lu, D.; Gao, X. Multi-objective optimization of gap-graded cement paste blended with supplementary cementitious materials using response surface methodology. *Constr. Build. Mater.* **2020**, *248*, 118552. [CrossRef]
48. Trincal, V.; Multon, S.; Benavent, V.; Lahalle, H.; Balsamo, B.; Caron, A.; Bucher, R.; Caselles, L.D.; Cyr, M. Shrinkage mitigation of metakaolin-based geopolymer activated by sodium silicate solution. *Cem. Concr. Res.* **2022**, *162*, 106993. [CrossRef]
49. Sánchez-Mendieta, C.; Galán-Díaz, J.J.; Martinez-Lage, I. Relationships between density, porosity, compressive strength and permeability in porous concretes: Optimization of properties through control of the water-cement ratio and aggregate type. *J. Build. Eng.* **2024**, *97*, 110858. [CrossRef]
50. Jamil, N.H.; Al Bakri Abdullah, M.M.; Pa, F.C.; Mohamad, H.; Ibrahim, W.M.A.W.; Chaiprapa, J. Influences of SiO_2, Al_2O_3, CaO and MgO in phase transformation of sintered kaolin-ground granulated blast furnace slag geopolymer. *J. Mater. Res. Technol.* **2020**, *9*, 14922–14932. [CrossRef]
51. Chen, C.; Liu, H.; Zhang, Y.; Gu, G.; Hu, J. Micro-assessment of heavy metal immobilization within alkali-activated copper tailings-slag geopolymer. *Cem. Concr. Compos.* **2024**, *149*, 105510. [CrossRef]
52. Zheng, Y.; Rao, F.; Yang, L.; Zhong, S. Comparison of ternary and dual combined waste-derived alkali activators on the durability of volcanic ash-based geopolymers. *Cem. Concr. Compos.* **2023**, *136*, 104886. [CrossRef]
53. Ruan, S.; Chen, S.; Lu, J.; Zeng, Q.; Liu, Y.; Yan, D. Waterproof geopolymer composites modified by hydrophobic particles and polydimethylsiloxane. *Compos. Part B Eng.* **2022**, *237*, 109865. [CrossRef]
54. Xie, J.; Wang, J.; Rao, R.; Wang, C.; Fang, C. Effects of combined usage of GGBS and fly ash on workability and mechanical properties of alkali activated geopolymer concrete with recycled aggregate. *Compos. Part B Eng.* **2019**, *164*, 179–190. [CrossRef]
55. Yang, S.; Guan, X.; Lu, J.; Cui, H.; Poon, C.S. Micromechanical and chemical characteristics of interfacial transition zone in alkali-activated slag concrete containing lightweight iron-rich aggregates. *Compos. Part B Eng.* **2024**, *283*, 111671. [CrossRef]
56. Zhang, W.; Liu, X.; Wang, Y.; Li, Z.; Li, Y.; Ren, Y. Binary reaction behaviors of red mud based cementitious material: Hydration characteristics and Na+ utilization. *J. Hazard. Mater.* **2021**, *410*, 124592. [CrossRef]
57. Han, Y.; Lin, R.; Lim, J.; Wang, X.-Y. Enhancing the properties of alkali-activated slag through dry ice addition: Investigation of hydration products and performance characteristics. *J. Mater. Res. Technol.* **2023**, *26*, 8983–8996. [CrossRef]
58. Sun, T.; Fan, J.; Ouyang, G.; Xu, F.; Wang, Z.; Yin, W.; Li, W. Alkali-activated slag mortar molded by non-stirring molding: Compressive strength, hydration properties and microstructures. *Case Stud. Constr. Mater.* **2023**, *18*, e02135. [CrossRef]
59. He, J.; Hu, T.; Sang, G.; Song, X.; Wu, Y.; Chen, Z. Effect of blended inorganic salts containing negative hydration ions on hydration and properties of alkali-activated slag cement. *Ceram. Int.* **2023**, *49*, 29553–29563. [CrossRef]
60. Wu, M.; Shen, W.; Xiong, X.; Zhao, L.; Yu, Z.; Sun, H.; Xu, G.; Zhao, Q.; Wang, G.; Zhang, W. Effects of the phosphogypsum on the hydration and microstructure of alkali activated slag pastes. *Constr. Build. Mater.* **2023**, *368*, 130391. [CrossRef]
61. Sandanayake, M.; Law, D.; Sargent, P. A new framework for assessing the environmental impacts of circular economy friendly soil waste-based geopolymer cements. *Build. Environ.* **2022**, *210*, 108702. [CrossRef]
62. Liu, J.; Gao, X.; Chen, T. Effect of SiO_2-modified calcined layered double hydroxides on the properties of cement-based material: Crucial role of the phase-transformation induced by alkaline pore solution. *Cem. Concr. Res.* **2024**, *178*, 107465. [CrossRef]
63. Sakulich, A.R. Reinforced geopolymer composites for enhanced material greenness and durability. *Sustain. Cities Soc.* **2011**, *1*, 195–210. [CrossRef]
64. Luo, Y.; Brouwers, H.J.H.; Yu, Q. Understanding the gel compatibility and thermal behavior of alkali activated class f fly ash/ladle slag: The underlying role of ca availability. *Cem. Concr. Res.* **2023**, *170*, 107198. [CrossRef]